Interlibrary Loans and Journal Article Requests

Notice Warning Concerning Copyright Restrictions:

The copyright law of the United States (Title 17, United States Code) governs the making of photocopies or other reproductions of copyrighted materials.

Under certain conditions specified in the law, libraries and archives are authorized to furnish a photocopy or other reproduction. One specified condition is that the photocopy or reproduction is not to be *"used for any purpose other than private study, scholarship, or research."* If a user makes a request for, or later uses, a photocopy or reproduction for purposes in excess of "fair use," that user may be liable for copyright infringement.

Upon receipt of this reproduction of the publication you have requested, you understand that the publication may be protected by copyright law. You also understand that you are expected to comply with copyright law and to limit your use to one for private study, scholarship, or research and not to systematically reproduce or in any way make available multiple copies of the publication.

The Stephen B. Thacker CDC Library reserves the right to refuse to accept a copying order if, in its judgment, fulfillment of the order would involve violation of copyright law.

Terms and Conditions for items sent by e-mail:

The contents of the attached document may be protected by copyright law. The CDC copyright policy outlines the responsibilities and guidance related to the reproduction of copyrighted materials at CDC. If the document is protected by copyright law, the following restrictions apply:

- You may print only one paper copy, from which you may not make further copies, except as maybe allowed by law.
- You may not make further electronic copies or convert the file into any other format.
- You may not cut and paste or otherwise alter the text.

ACS Biomaterials SCIENCE & ENGINEERING

pubs.acs.org/journal/abseba

Article

SOX2Mediates Carbon Nanotube-Induced Fibrogenesis and Fibroblast Stem Cell Acquisition

Chayanin Kiratipaiboon, Maria Voronkova, Rajib Ghosh, Liying W. Rojanasakul, Cerasela Zoica Dinu, Yi Charlie Chen, and Yon Rojanasakul*

Cite This: *ACS Biomater. Sci. Eng.* 2020, 6, 5290−5304

Read Online

ACCESS | Metrics & More | Article Recommendations | Supporting Information

ABSTRACT: Certain nanosized particles like carbon nanotubes (CNTs) are known to induce pulmonary fibrosis, but the underlying mechanisms are unclear, and efforts to prevent this disease are lacking. Fibroblast-associated stem cells (FSCs) have been suggested as a critical driver of fibrosis induced by CNTs by serving as a renewable source of extracellular matrix-producing cells; however, a detailed understanding of this process remains obscure. Here, we demonstrated that single-walled CNTs induced FSC acquisition and fibrogenic responses in primary human lung fibroblasts. This was indicated by increased expression of stem cell markers (e.g., CD44 and ABCG2) and fibrogenic markers (e.g., collagen and α-SMA) in CNT-exposed cells. These cells also showed increased sphere formation, anoikis resistance, and aldehyde dehydrogenase (ALDH) activities, which are characteristics of stem cells. Mechanistic studies revealed sex-determining region Y-box 2 (SOX2), a self-renewal associated transcription factor, as a key driver of FSC acquisition and fibrogenesis. Upregulation and colocalization of SOX2 and COL1 were found in the fibrotic lung tissues of CNT-exposed mice via oropharyngeal aspiration after 56 days. The knockdown of SOX2 by gene silencing abrogated the fibrogenic and FSC-inducing effects of CNTs. Chromatin immunoprecipitation assays identified SOX2-binding sites on *COL1A1* and *COL1A2*, indicating SOX2 as a transcription factor in collagen synthesis. SOX2 was also found to play a critical role in TGF-β-induced fibrogenesis through its collagen- and FSC-inducing effects. Since many nanomaterials are known to induce TGF-β, our findings that SOX2 regulate FSCs and fibrogenesis may have broad implications on the fibrogenic mechanisms and treatment strategies of various nanomaterial-induced fibrotic disorders.

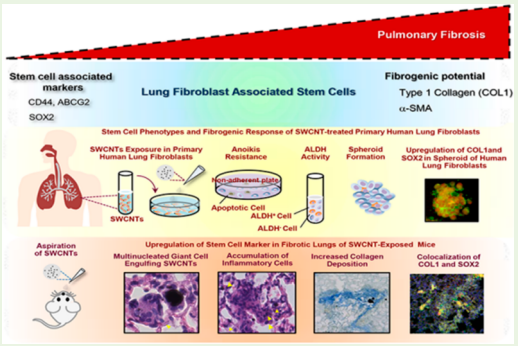

KEYWORDS: *nanomaterial, fibrogenicity, myofibroblasts, self-renewal*

1. INTRODUCTION

Due to several unique and desirable properties, such as high tensile strength and electrical conductivity, carbon nanotubes (CNTs), a group of engineered carbonaceous nanomaterials, are used in various commercial and industrial applications.[1−4] In addition, their near-infrared absorption and photoemission characteristics are being explored for various biomedical applications such as photothermal therapy and bioimaging.[5−8] The increased use of CNTs implicates a heightened risk of human exposure and adverse health consequences, partly due to their biological activities and persistence,[9−11] which have increasingly been reported. Inhaled CNTs can reach the interstitial alveolar region and remain trapped for an extended period of time due to impaired phagocytic clearance by macrophages,[12−16] leading to chronic diseases such as pulmonary fibrosis.[17,18]

Acute CNT exposure has been reported to induce pulmonary cell infiltration and cytokine release giving rise to inflammatory responses in the lungs;[19−21] therefore, it has been used as a predictive model for mechanistic investigations of fiber-induced lung inflammation.[22] Recent studies have indicated that alveolar retention of CNTs may span over 100 days after initial exposure.[16,23,24] This could lead to impaired clearance of CNTs by alveolar macrophages as a foreign agent, which results in the accumulation of CNTs in lung interstitium.[13,25−27] Numerous in vivo experiments have also demonstrated that exposure to CNTs at physiologically relevant concentrations via inhalation, intratracheal instillation, or pharyngeal aspiration caused acute inflammatory responses and chronic pulmonary fibrosis characterized by increased collagen deposition, epithelioid granulomas formation, and fibrotic scarring of the lungs.[12,26,28−30] Moreover, in vitro studies showed that CNTs could promote fibroblast cell proliferation, collagen production, and release of various

Received: June 13, 2020
Accepted: August 11, 2020
Published: August 11, 2020

https://dx.doi.org/10.1021/acsbiomaterials.0c00887
ACS Biomater. Sci. Eng. 2020, 6, 5290−5304

fibrogenic cytokines such as transforming growth factor-beta (TGF-β) and matrix metalloproteinase (MMP)-9.[31−33]

Pulmonary fibrosis occurs as a result of lung damage and excessive accumulation of extracellular matrix (ECM) in the damaged tissues that develop over time. In this process, activation of ECM-producing fibroblasts and myofibroblasts is generally considered as an initial event.[34] Such activation is usually a result of chronic tissue injury and inflammation that causes the transformation of fibroblasts into myofibroblasts, which is characterized by alpha-smooth muscle actin (α-SMA).[35,36] Uncontrolled growth and proliferation of these cells can result in excessive ECM accumulation, which creates deformation in tissue structures followed by a diminution in whole organ function.[37,38] Evolving research indicates that stem cells may bring forth active fibroblasts and myofibroblasts during fibrogenesis since a subpopulation of cells expressing self-renewal related transcription factors like POU class 5 homeobox 1 (OCT4), Nanog homeobox (NANOG), and SRY-box transcription factor 2 (SOX2), has been observed in fibroblastic lesions of various fibrotic tissues,[39−43] although their precise role in fibrogenesis remains obscure.

Recent studies by our group also showed that CNT exposure could transform normal human lung fibroblasts (NHLFs) toward stem cells or stem-like cells.[32,44] These fibroblast-associated stem cells (FSCs) are capable of forming collagen-rich fibroblastic foci similar to those noticed in animal models and patients with pulmonary fibrosis.[32,44] In patients, the formation of fibroblastic foci has commonly been used as a reliable marker of poor prognosis.[45,46] Such structures have also been shown to be induced by CNTs. They contain high levels of collagen and stem cell markers such as aldehyde dehydrogenase (ALDH) activity, ATP binding cassette subfamily G member 2 (ABCG2), and CD90 based on our previous studies.[32,44] Animal studies also showed the overexpression of these stem cell-related markers in fibrotic lesions of CNT-exposed lungs.[44] Together, these studies suggest the putative role of FSCs in CNTmediated fibrosis, but the underlying mechanisms of FSC induction and its role in fibrogenesis remain to be investigated.

2. MATERIALS AND METHODS

2.1. Nanomaterial Characterization. SWCNTs were obtained from NanoLab, Inc. (Waltham, MA, U.S.A.) and were characterized for particle dimension, hydrodynamic size, zeta potential, and chemical composition. Particle dimensions were assessed by electron microscopy, as previously described.[31] Dynamic light scattering (DLS) method was used to measure the hydrodynamic diameter of particles using NanoSight NS300 (Malvern Instrument, Worcestershire, U.K.). SWCNT particles were dispersed in sterile water at a concentration of 10 mg mL^{-1} as a stock suspension. The suspension was subsequently diluted into 1 mg mL^{-1} of 0.5% bovine serum albumin (BSA) in Ca^{2+} and Mg^{2+}-free phosphate-buffered saline (dPBS). The suspension was then further diluted into 0.1 mg mL^{-1} using a premixed complete fibroblast cell culture medium (FBM). For characterization of SWCNTs in dispersion medium (DM), particles were dispersed in DM containing 0.01 mg mL^{-1} 1,2-dipalmitoyl-*sn*-glycero-3-phosphocholine, 5.5 mM D-glucose, and 0.6 mg mL^{-1} mouse serum albumin in dPBS at a concentration of 0.1 mg mL^{-1}. Furthermore, 0.1 mg mL^{-1} SWCNTs in sterile water or dPBS containing 0.5% BSA were also prepared from the SWCNT stock suspension. DLS measurements of each SWCNT suspension were performed using an argon ion laser at an excitation wavelength of 488 nm, with a scattering angle of 90° and at the particle concentration of 0.1 mg mL^{-1}. Measurements of zeta potential were conducted by Zetasizer Nano ZS90 (Malvern Instrument). After an initial 2 min equilibration of each SWCNT suspension in the instrument, five measurements with a 10-s delay between measurements and each consisting of five runs with a 2-s delay between runs were recorded. The Fourier transform infrared spectroscopy (FTIR) spectroscopy was used to assess the chemical composition of SWCNTs. FTIR analysis in the 500−4000 cm^{-1} region was carried out in an FTS 7000e Varian FTIR spectrometer (Varian Medical Systems, Palo Alto, CA, U.S.A.) using the KBr pellet technique. All spectra were evaluated according to the catalog of Spectrometric Identification of Organic Compounds.[47] Elemental carbon of our sample was analyzed using energy dispersive X-ray spectrum (EDX).

2.2. Cell Culture and Transfection. Normal human lung fibroblasts (NHLFs) from the American Type Culture Collection (Manassas, VA, U.S.A.) were used throughout this study. They were cultured in complete FBM medium with Fibroblast Growth Medium-2 SingleQuots supplemented with 2% fetal bovine serum (FBS), 0.1% insulin, 0.1% human basic fibroblast growth factor (bFGF), 30 μg mL^{-1} gentamicin, and 15 ng mL^{-1} amphotericin (Lonza Walkersville, Inc., Walkersville, MD, U.S.A.). The cells were maintained under a subconfluence condition at 37 °C with 5% CO_2. Early passages of NHLFs (passages 2−5) were used in this study. For the generation of stable SOX2 knockdown cells, 2×10^5 cells were seeded in each well of 6-well plates with a total volume of 1 mL of media and incubated overnight. SOX2 knockdown experiments were conducted using lentivirus-mediated gene transfection. The cells were washed, and the culture medium was replaced with 2.5 mL per well of fresh medium containing 2 μg mL^{-1} hexadimethrine bromide. The cells were then infected with either control or SOX2 shRNA lentivirus (Applied Biological Materials Inc., Richmond, BC, Canada) and incubated for 24 h. Next, the cell culture medium was replaced with 2 mL of fresh medium, and cells were further cultured for 48 h and allowed to recover for 24 h prior to experiments.

2.3. Animals. All animal studies were conducted using six-week-old male C57BL/6J mice from Jackson Laboratories (Bar Harbor, ME, USA). The animals were contained in an AAALAC accredited, pathogen-free environment with free access to water and food. They were adjusted for 1 week prior to any experimental procedures. All animal care and experimental procedures were performed following the Guidelines for Animal Experiments at West Virginia University and Institutional Animal Care and Use Committee (IACUC #1512000008.1) approved protocol.

2.4. Oropharyngeal Aspiration of Nanoparticles. Preparation of SWCNT suspensions for oropharyngeal aspiration was performed as previously described by Wang et al.[31] Briefly, particles were dispersed in sterile DM by sonication using Branson 450 digital sonifier (Marshall Scientific, Hampton, NH, U.S.A.) at the setting of 10 W output and 50% duty cycle for 5 min. Freshly prepared suspensions of SWCNT were used in all studies. For aspiration, animals were anesthetized by isoflurane (Abbott Laboratories, North Chicago, IL, U.S.A.) and positioned by holding the incisor teeth with a surgical thread against their back on a slant supporting board. The tongue was pulled gently and held with forceps, DM control, or DM containing 40 μg of SWCNT at a volume of 40 μL was administered to the oropharynx at tongue base. The tongue was held for approximately 10 s or until a few deep breaths were completed. The mouse was then returned to its cage, laid on its left side, and allowed to recover from the aspiration procedure.

2.5. SWCNT Preparation for In Vitro Studies. For in vitro experiments, SWCNT stock suspension (10 mg mL^{-1}) in sterile water was diluted into 1 mg mL^{-1}. The suspension was further diluted into 0.1 mg mL^{-1} of 0.5% BSA in dPBS solution as a stock and kept at 4 °C. Prior to use, the SWCNT preparation was sonicated 3 times, for 10 s each, at 5 W output, and 30% duty cycle using Hielscher UIS259L sonicator (Ringwood, NJ, U.S.A.).

2.6. Cell Proliferation. For cell proliferation assays, 1×10^4 cells per well were seeded in 96-well plates (Fisher, Waltham, MA, U.S.A.) and incubated for 16 h. They were treated with different concentrations of SWCNTs for 48 h. Cell proliferation was evaluated by 3-(4,5-dimethylthiazol-2-yl)-2,5-diphenyltetrazolium (MTT) assay. After treatments, cells were incubated with 500 μg mL^{-1}

https://dx.doi.org/10.1021/acsbiomaterials.0c00887
ACS Biomater. Sci. Eng. 2020, 6, 5290−5304

MTT (Invitrogen, Carlsbad, CA, U.S.A.) for 4 h at 37 °C. Cell proliferation was determined spectrophotometrically by measuring the formazan product at 570 nm using a microplate reader (Anthos, Durham, NC, U.S.A.).

2.7. Immunoblotting. In each well of 6-well plates, 1.5×10^5 cells were plated and incubated for 16 h, after which they were exposed to different concentrations of SWCNTs for 48 h. The cells were harvested and prepared for immunoblotting analysis by incubating for 30 min with a lysis buffer containing 2% Triton X-100, 100 mM NaCl, 10 mM Tris-HCl (pH 7.5), 1% sodium dodecyl sulfate (SDS), 1 mM EDTA, and a Complete cocktail protease inhibitors (Roche Molecular Biochemicals, Basel, Switzerland). Protein content was determined by Bradford assay using a commercial kit from Bio-Rad Laboratories (Hercules, CA, U.S.A.). Lysate proteins were denatured and equal amounts of the proteins (20 μg) were resolved on 10% SDS-polyacrylamide gel electrophoresis (SDS-PAGE) and electrophoretically transferred onto nitrocellulose membranes (Bio-Rad). The membranes were blocked with 5% nonfat dry milk in Tris-buffered saline with Tween 20 (TBST) for 1 h and incubated overnight with primary antibodies against type 1 collagen (COL1; GeneTex, Inc., Irvine, CA, U.S.A.), α-SMA, ABCG2, CD44, NANOG, OCT4, and SOX2 (Cell Signaling Technology, Danvers, MA, U.S.A.) at 4 °C. After incubation, the membranes were washed with TBST and further incubated with horseradish peroxidase-labeled secondary antibodies for 2 h at room temperature. The immune complexes were analyzed by an enhanced chemiluminescence (ECL) detection system (Millipore Corporation, Billerica, MA, U.S.A.), and the luminescence signals were quantified using ImageJ.

2.8. Tissue Processing. The animals were euthanized after the experiments, and the lungs were fixed with 1 mL of 10% neutral buffered formalin by intratracheal perfusion via a tracheal cannula. After fixation, the lungs were sliced into tissue blocks (2−3 mm thick) to embed in paraffin. Sections (5 μm thick) were then cut and stained with Mayer's hematoxylin (Sigma-Aldrich, St. Louis, MO, U.S.A.). The deposition of collagen was detected by aniline blue (Sigma-Aldrich) and Sirius red (American Mastertech Scientific, Inc., Lodi, CA, U.S.A.) staining. Lung tissue sections were mounted and visualized on a light microscope.

2.9. Sphere Formation Assay. Sphere formation assay was performed following the protocol detailed elsewhere.[48] Briefly, cells were suspended in serum-free medium containing 0.8% methyl-cellulose supplemented with 20 ng mL^{-1} EGF (BD Biosciences, San Jose, CA, U.S.A.), 4 μg mL^{-1} bFGF, and insulin (Sigma-Aldrich). Then 3×10^4 cells per well in a total volume of 400 μL with matrigel were seeded onto an ultralow attachment 24-well plate and incubated with different concentrations of SWCNTs for 14 days. The culture medium was replaced every 3 days with the same methyl cellulose-containing serum-free medium supplemented with growth factors as described above.

2.10. Immunofluorescence. NHLF cells were seeded on coverslips, fixed with 4% paraformaldehyde, and permeabilized with 0.25% Triton-X for 10 min at room temperature, as previously described.[48] The cells were subsequently blocked with 1.5% goat serum, 1% FBS and 0.5% saponin, and incubated overnight with primary antibodies against COL1 (1:200) from GeneTex, Inc., α-SMA (1:500) and SOX2 (1:400) from Cell Signaling Technology at 4 °C. The cells were incubated with AlexaFluor 488 and 647-conjugated secondary antibodies (1:500; Thermo Fisher Scientific, Waltham, MA, U.S.A.) at room temperature for 1 h with gentle rocking. Finally, coverslips were mounted on glass slides using diamidino phenylindole (DAPI)-containing medium (Vector Laboratories Inc., Burlingame, CA, U.S.A.), imaged using a Keyence BZ-X700 fluorescence microscope (Itasca, IL, U.S.A.) and analyzed with ImageJ. For paraffin-embedded mouse lung tissue sections, deparaffinized slides were subjected to antigen retrieval in citrate buffer at 120 °C for 20 min. They were washed twice with a permeabilization buffer containing 1% BSA in PBS with 0.4% Triton X-100 (PBST) for 10 min and blocked with 5% goat serum in PBST for 30 h. Tissue slides were subsequently incubated with primary, fluorescently conjugated secondary antibodies, mounted, and analyzed using the same procedure described above.

2.11. ALDH Activity. ALDH activity was measured using the Aldefluor assay kit (Stem Cell Technologies) following manufacturer's instructions. In brief, 9×10^5 cells were seeded in 100 mm culture dishes and incubated for 16 h. NHLF cells were then treated with various doses of SWCNTs for 48 h at a total volume of 12 mL. After specified treatment durations, 1×10^6 cells were collected, processed, and suspended in 1 mL Aldefluor buffer containing activated Aldefluor substrate in the presence or absence of diethylaminobenzaldehyde (DEAB), a specific ALDH inhibitor, for 45 min at 37 °C. The cells were then centrifuged and suspended in the Aldefluor buffer and ALDH activity was determined using BD Fortessa cell analyzer (BD Biosciences, San Jose, CA, U.S.A.). Raw flow cytometry data were exported using FCS Express 6 software (De novo software, pasadena, CA, U.S.A.) for further analysis.

2.12. Anoikis and Apoptosis Assays. Anoikis and apoptosis assays were performed according to the methods previously described with minimal modifications.[48] Briefly, 1.5×10^5 NHLF cells were seeded in each well of 6-well plates and incubated overnight. The cells were then treated with SWCNTs in a total volume of 2 mL in complete FBM for 48 h. After the treatment, cells were detached, collected, replated in 6-well ultralow attachment plates, and analyzed for anoikis and apoptosis following the published protocol.[48]

2.13. Chromatin Immunoprecipitation. Chromatin immunoprecipitation (ChIP-PCR) was carried out using Simple ChIP plus Enzymatic Chromatin IP Kit (Cell Signaling: #9005) following the manufacturer's instructions. In summary, 5×10^6 cells were plated in a 100 mm culture dish with 7 mL of complete FBM and cultured for 16 h. Following whole-cell cross-linking with 1% formaldehyde and lysis, the nuclear pellet was digested by Micrococcal nuclease and sonicated to achieve desired chromatin fragmentation. The resulting chromatin−protein complexes were incubated with anti-SOX2 antibody (Cell Signaling Technology) or negative control IgG (Vector Laboratories) overnight. After immunoprecipitation, protein G magnetic beads (50 μL) were added and incubated and the antibody complexes were incubated at 65 °C overnight for reverse cross-linking. The purified DNA was then collected, and the relative enrichment of specific regions in ChIP-DNA was determined using SYBR Green Master Mix (Applied Biosystems) in an ABI 7500 Real-Time PCR (Applied Biosystems). Primer oligonucleotides used in the ChIP study are shown in the Supporting Information, Table S3.

2.14. Double Immunofluorescence for Flow Cytometry Analysis. NHLF cells were seeded and treated with SWCNTs as described in section 2.7. After the treatment, cells were collected, fixed in 4% paraformaldehyde solution for 15 min, and permeabilized in ice-cold methanol with gentle vortexing for 30 min. The cells were then incubated with a mixture of primary antibodies against SOX2 (1:300; Cell Signaling Technology) and COL1 (1:200; GeneTex, Inc.) overnight at 4 °C. After three washes with PBST, cells were incubated for 1 h with the mixture of AlexaFluor 488 and 647-conjugated secondary antibodies (1:500; Thermo Fisher Scientific) at room temperature. Subsequently, the cells were washed three times with PBST, suspended in cold PBS, and ran on BD Fortessa instrument (BD Biosciences). FCS Express 6 was used to export raw data from the flow cytometer for analysis.

2.15. Statistical Analysis. Data were represented as means ± SD from at least three independent experiments unless otherwise mentioned. Statistical significance was determined using a student's *t*-test, two-way ANOVA, and post hoc Tukey's test for multiple comparisons at a significance level (α) of 0.05. The relationship between SOX2 and collagen expression was determined by Pearson's correlation coefficient analysis.

3. RESULTS AND DISCUSSION

3.1. CNT Characterization. All SWCNTs used in this study were characterized by various microscopic and spectroscopic techniques as summarized in Table 1. Scanning electron microscopic (SEM) analysis showed individual

https://dx.doi.org/10.1021/acsbiomaterials.0c00887
ACS Biomater. Sci. Eng. 2020, 6, 5290−5304

Table 1. Physicochemical Properties of SWCNTs Used in This Study[a]

properties	SWCNT
dry mean width (nm)	1.5
dry mean length (μm)	1−5
aspect ratio	600−3,000
hydrodynamic diameter (nm)	95.6 + 42.9[1]
hydrodynamic diameter (nm)	107.2 ± 47.5[2]
zeta potential (mV)	−9.96 ± 0.42[1]
zeta potential (mV)	−5.67 ± 0.95[2]
% carbon (w/w)	∼98%

[a]Superscript "1" and "2" represent hydrodynamic diameter or zeta potential of SWCNTs 0.1 mg mL^{-1} in cell culture medium and dispersion medium, respectively.

nanotubes forming bundles in a rope-like structure (Figure 1a) with an average length of 1−5 μm, a width (diameter) of 1.5 nm, and mean aspect ratio of 600−3000. The hydrodynamic diameter of SWCNTs (Table 1) in sterile water, 0.5% BSA in dPBS, cell culture medium and DM was determined by dynamic light scattering (DLS) and was found to be 207.5 ± 82 (Table S1), 126.1 ± 69.1 (Table S1), 95.6 ± 42.9, and 107.2 ± 47.5 nm, respectively. An average hydrodynamic diameter of SWCNTs obtained from DLS measurements clearly indicated agglomeration of SWCNT particles in the suspending media. The results further suggested that SWCNTs were less agglomerated in cell culture medium and DM, likely as a result of fetal bovine serum (FBS) and dispersants (1,2-dipalmitoyl-*sn*-glycero-3-phosphocholine and mouse serum albumin) as compared to sterile water, although the results should be interpreted with caution since DLS measurements of nonspherical objects may be imprecise. The surface charge of SWCNTs (Table 1) in the dispersion media was −12.83 ± 1.58 (Table S1), −9.88 ± 1.09 (Table S1), −9.96 ± 0.42, and −5.67 ± 0.95 mV, respectively. The structure and purity of SWCNTs were assessed using Fourier-transform infrared spectroscopy (FTIR). FTIR spectra of the nanopartcles (Figure 1b) revealed a peak at 3436 cm^{-1}, which is characterized by the stretching vibration of −OH groups. Two smaller peaks at 2915 and 2848 cm^{-1} are allotted to C−H stretching vibrations.[49] Aromatic C=C stretching vibrations were observed at 1650 and 1400 cm^{-1}. The energy dispersion spectroscopy (EDS) spectrum revealed the presence of carbon up to approximately 98% in the tested samples (see Supporting Information, Figure S1 for EDS analysis). The observed FTIR and EDS spectra confirmed the chemical identity and purity of the tested SWCNT particles.

3.2. SWCNTs Induce Fibrogenic Response in NHLFs and Mice. Prior to determining the fibrogenic activity of SWCNTs in NHLFs, noncytotoxic concentrations of CNTs in the tested lung cells were first determined by MTT assay. Treatment of NHLFs with different surface area concentrations of SWCNTs (0−1.6 μg cm^{-2} or 0−7.60 μg mL^{-1}; see Supporting Information, Table S2 for in vitro doses) for 2 days caused a slight increase in cell proliferation at low concentrations (≤0.2 μg cm^{-2} or ≤0.95 μg mL^{-1}), but a decrease in proliferation at high concentrations (≥0.4 μg cm^{-2} or ≥1.90 μg mL^{-1}), which is likely due to cellular toxicity (Figure 2a). To determine the fibrogenic activity of SWCNTs, noncytotoxic concentrations of SWCNTs (0.05, 0.1, and 0.2 μg cm^{-2} or 0.24, 0.47, and 0.95 μg mL^{-1}) were used to treat NHLFs and their effects on type 1 collagen (COL1) and α-SMA expression were evaluated by Western blotting. These concentrations are physiologically relevant based on the reported *in vivo* fibrogenic doses of 40−80 μg in mice,[27] which is equivalent to the in vitro surface area dose of 0.08−0.16 μg cm^{-2}, assuming an average mouse alveolar surface area of 500 cm^2.[50] Figure 2b,c shows that treatment of NHLFs with SWCNTs strongly upregulated the expression levels of COL1 and α-SMA. Furthermore, we assessed the effects of SWCNT treatment on pro-fibrotic cytokine TGF-β and matrix metalloproteinases (MMPs) such as MMP2 and MMP9, which are known to enhance fibrosis.[51,52] Figure S2a,b shows that SWCNT treatment had no significant effect on MMP2 expression but substantially upregulated the expression of TGF-β and MMP9 as compared to the untreated control. MMP9 was reported to induce α-SMA expression, which indicates myofibroblast differentiation possibly as a result of TFG-β activation.[53] Analysis of collagen accumulation with aniline blue and Sirius red staining assays further supports the induction of collagen production by SWCNTs (Figure 2d−f). In vivo studies showed an accumulation of inflammatory cells, including macrophages and neutrophils in the lungs of SWCNT-treated mice at 7 days postexposure (Figure 3a). At 56 days postexposure, thickening of the alveolar wall (Figure 3a) and increased collagen deposition in the mouse lungs were evident as indicated by aniline blue and Sirius red collagen staining (Figure 3b−e). These results indicate initial lung inflammation and subsequent lung fibrosis after exposure to SWCNTs.

3.3. SWCNTs Induce Stem Cell Phenotypes in NHLFs. Although their precise role in fibrogenesis has not been demonstrated, stem cells have been reported to be localized in the fibrotic lesions of various tissues. They are proposed to be an important source of ECM-producing cells.[32,40,41,43,44,54]

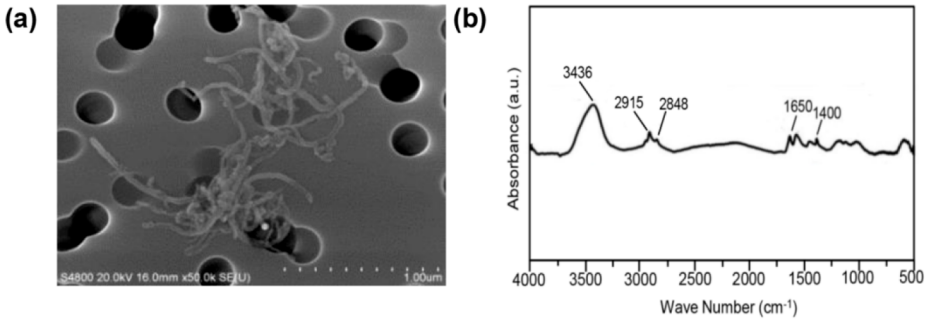

Figure 1. Characterization of SWCNTs. (a) Scanning electron micrograph of SWCNTs used in this study. (b) FTIR spectra of SWCNTs.

https://dx.doi.org/10.1021/acsbiomaterials.0c00887
ACS Biomater. Sci. Eng. 2020, 6, 5290−5304

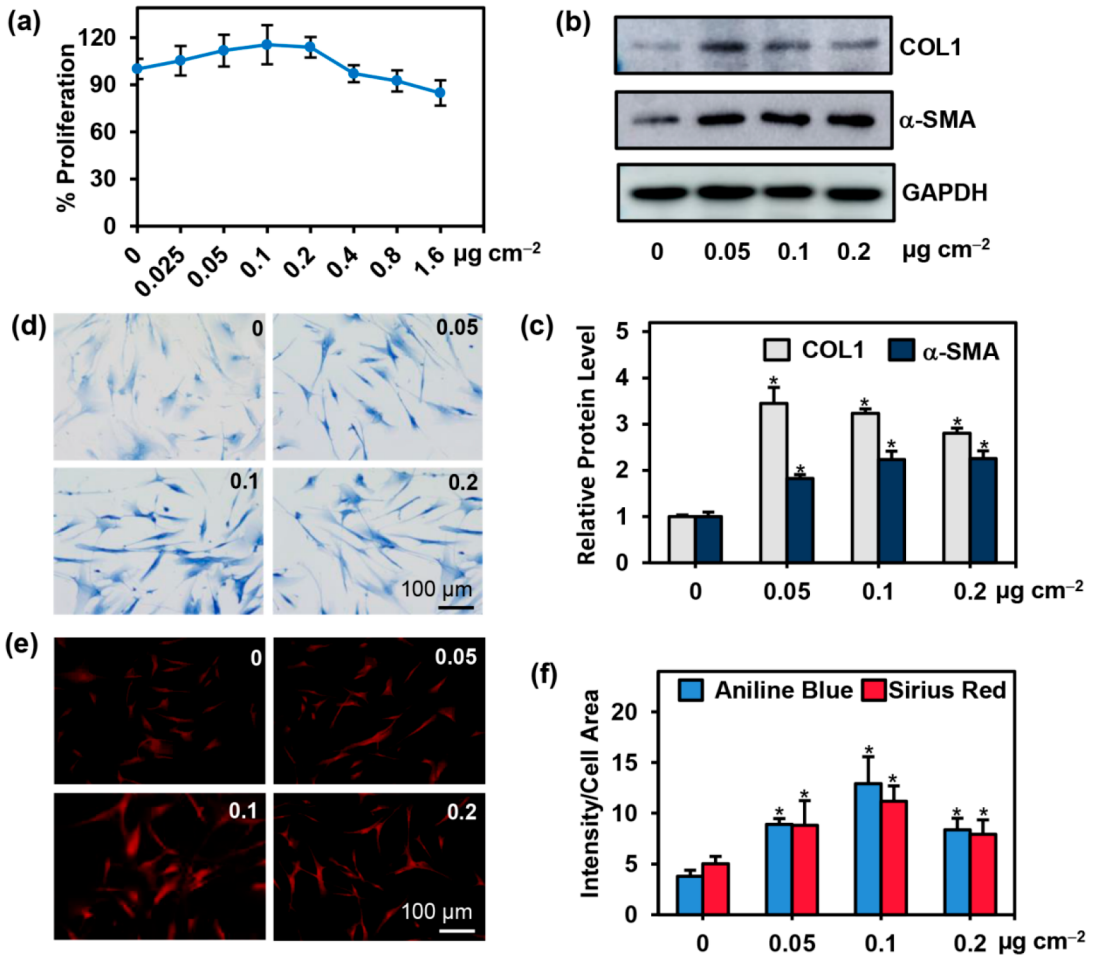

Figure 2. Induction of collagen expression by SWCNTs in human lung fibroblasts. Primary NHLF cells were exposed to various surface area concentrations (0−1.6 μg cm^{-2} or 0−7.6 μg mL^{-1}) of SWCNTs for 48 h. (a) Analysis of cell proliferation and cytotoxicity by MTT assay. (b) Immunoblot analysis of type 1 collagen and α-SMA proteins. GAPDH was used as a loading control. (c) Quantitative analysis of the protein expression in panel b. (d−f) Representative images and quantification of collagen with aniline blue and Sirius red staining. 200× magnification. The scale bar is 100 μm. Data presented as mean ± SD (n = 3), *p < 0.05 versus control cells.

Stem cells possess self-renewal properties and are capable of proliferating and forming spheroids under nonadherent conditions in serum-free media.[55] In this study, we assessed the stem properties of SWCNT-treated NHLFs using spheroid formation and anoikis (detachment-induced apoptosis) resistance assays. In the former assay, cells were seeded at a low density on nonadherent tissue culture plates and allowed to form spheroids in serum-free media with or without SWCNTs for 14 days. Figure 4a,b shows that treatment of the cells with SWCNTs significantly induced sphere formation as compared to the untreated control. Subsequently, the spheroids were collected and analyzed for collagen expression by a colorimetric Sircol assay. Figure 4c shows that spheroid-forming cells from SWCNT-treated NHLFs produced more soluble collagen than the untreated control. Immunofluorescence staining studies showed an increased expression of COL1 and α-SMA in SWCNT-treated spheroid cells as compared to untreated control (Figure 4d−g), suggesting the role of FSCs in SWCNT-induced fibrogenesis. We next assessed ALDH activity in these cells since ALDH has been widely used as a functional stem cell marker,[56] especially for cancer stem cells due to their ability to metabolize toxic aldehydes and resist cell death from chemotherapy.[57] ALDH has also been linked to fibrosis since the expression and activity of this enzyme were shown to be upregulated in fibroblasts from patients with conjunctiva fibrosis.[58] Furthermore, ALDH inhibitors such as disulfiram and DEAB inhibited collagen production in conjunctival fibrosis and prevented ovalbumin-induced conjunctiva fibrosis in a mouse model. In this study, we observed a higher ALDH activity in SWCNT-treated fibroblasts as compared to control untreated fibroblasts (Figure 5a,b), supporting the stem properties of SCNT-treated cells.

We also conducted an anoikis assay to validate the stem properties of SWCNT-treated cells. In this assay, cells were harvested as a single-cell suspension in serum-free medium and incubated in nonadherent cell culture plates for 36 h. The ability of cells to survive under these nonadherent conditions, which is a characteristic of stem cells, was then assessed by MTS assay. The result of this study shows that SWCNT-treated cells were able to survive and retain their viability better than the untreated control (Figure 5c). Hoechst 33342 apoptosis assay further confirmed the finding by demonstrating more apoptotic cell death in the control cells compared to SWCNT-treated cells (Figure 5d,e). These results indicate anoikis resistant phenotype and stem properties of SWCNT-treated cells.

3.4. SWCNTs Upregulate Stem Cell Markers in NHLFs.

A growing number of studies indicate the association between

https://dx.doi.org/10.1021/acsbiomaterials.0c00887
ACS Biomater. Sci. Eng. 2020, 6, 5290−5304

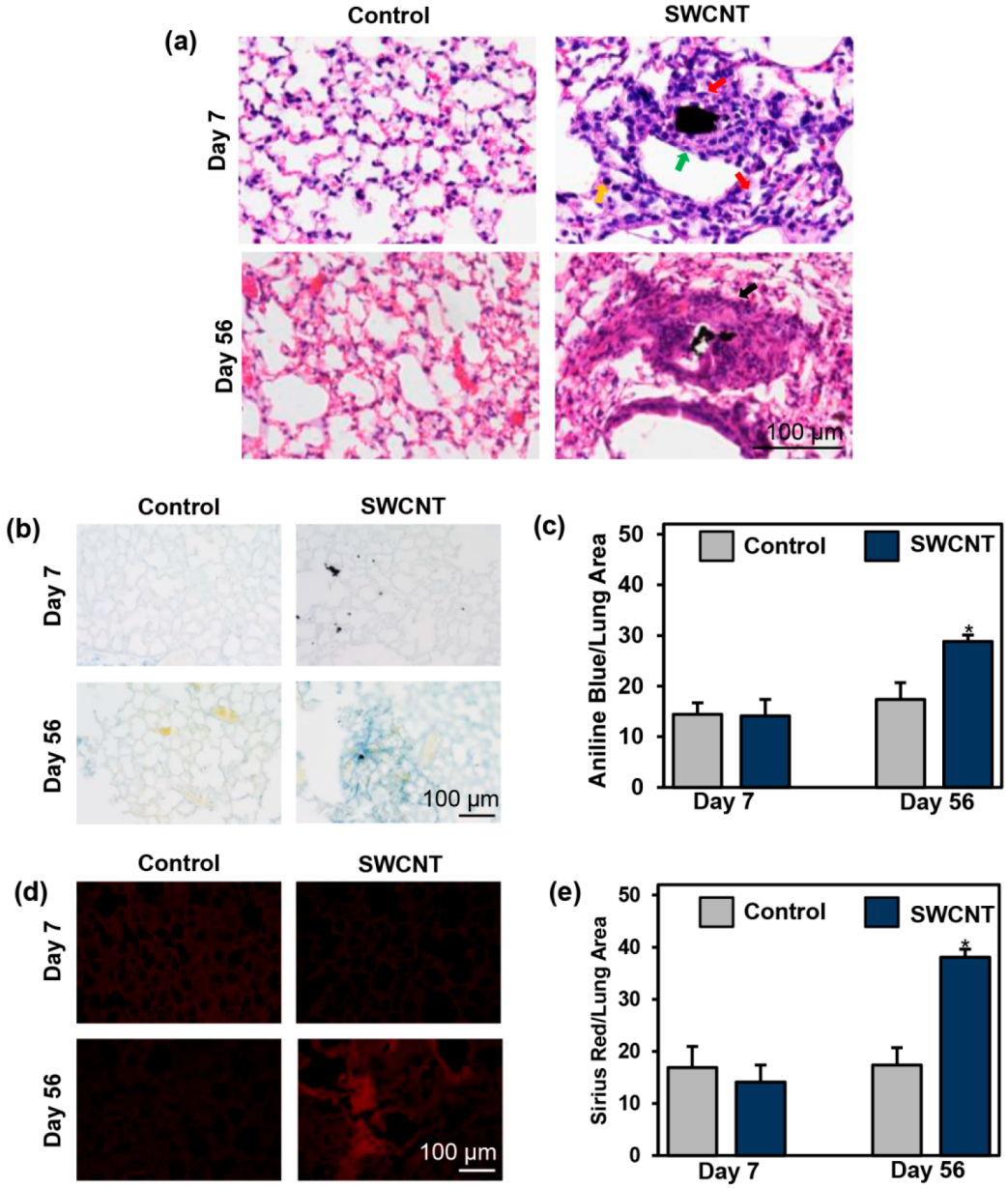

Figure 3. Induction of collagen expression by SWCNTs in mouse lung tissues. (a) H&E staining of lung tissue sections of mice treated with 0 or 40 μg of SWCNTs at 7 days and 56 days post-treatment. Yellow, red, green, and black arrows indicate macrophages, neutrophils, granuloma formation, and alveolar wall thickening. The scale bar is 100 μm. 400× magnification. (b,c) Representative images and quantification of collagen content by aniline blue staining at 7 days and 56 days post-treatment. (d,e) Representative images and quantification of collagen content by Sirius red staining at 7 days and 56 days post-treatment. The scale bar is 100 μm. 200× magnification. Data presented as mean ± SD ($n = 3$), *$p < 0.05$ versus control cells.

stem cell markers expression (e.g., CD44 and ABCG2) and fibrogenic responses in various fibrotic diseases.[59−63] In this study, we evaluated the possible connection between FSC induction and fibrogenic responses in SWCNT-treated NHLFs by analyzing stem cell markers expression by Western blotting. Figure 6a,b shows a substantial upregulation of CD44 and ABCG2 in NHLFs in response to SWCNT treatment. CD44 is a standard mesenchymal stem cell marker, and its expression has been associated with wound healing and fibrogenesis.[60,62,63] Knockout of CD44 in a mouse model of arteriovenous fistulae (AVF) resulted in a reduction of collagen deposition in AVF area.[63] In cardiac fibrosis, the treatment of fibroblasts with TGF-β promoted collagen production and differentiation of fibroblasts into myofibroblasts, the effects that can be prevented by an anti-CD44 antibody.[62] The role of CD44 in fibrogenesis is supported by the suppressive effect of CD44-neutralizing antibody on collagen production in TGF-β overexpressing mice.[62] In pulmonary fibrosis, CD44 was found to be upregulated in an animal model of bleomycin-induced fibrosis and its inhibition by neutralizing antibody or genetic ablation reduced the fibrogenic effect.[60]

ABCG2 belongs to the ATP-binding cassette (ABC) transporter protein family that is widely used as a universal stem cell marker.[64] The presence of ABCG2 positive cells has been identified in the injured and remodeled tissues of fibrotic lungs in bleomycin-treated mice. These cells subsequently acquired myofibroblast phenotype as identified by contractile characteristics and α-SMA expression.[61] In a mouse model of

https://dx.doi.org/10.1021/acsbiomaterials.0c00887
ACS Biomater. Sci. Eng. 2020, 6, 5290−5304

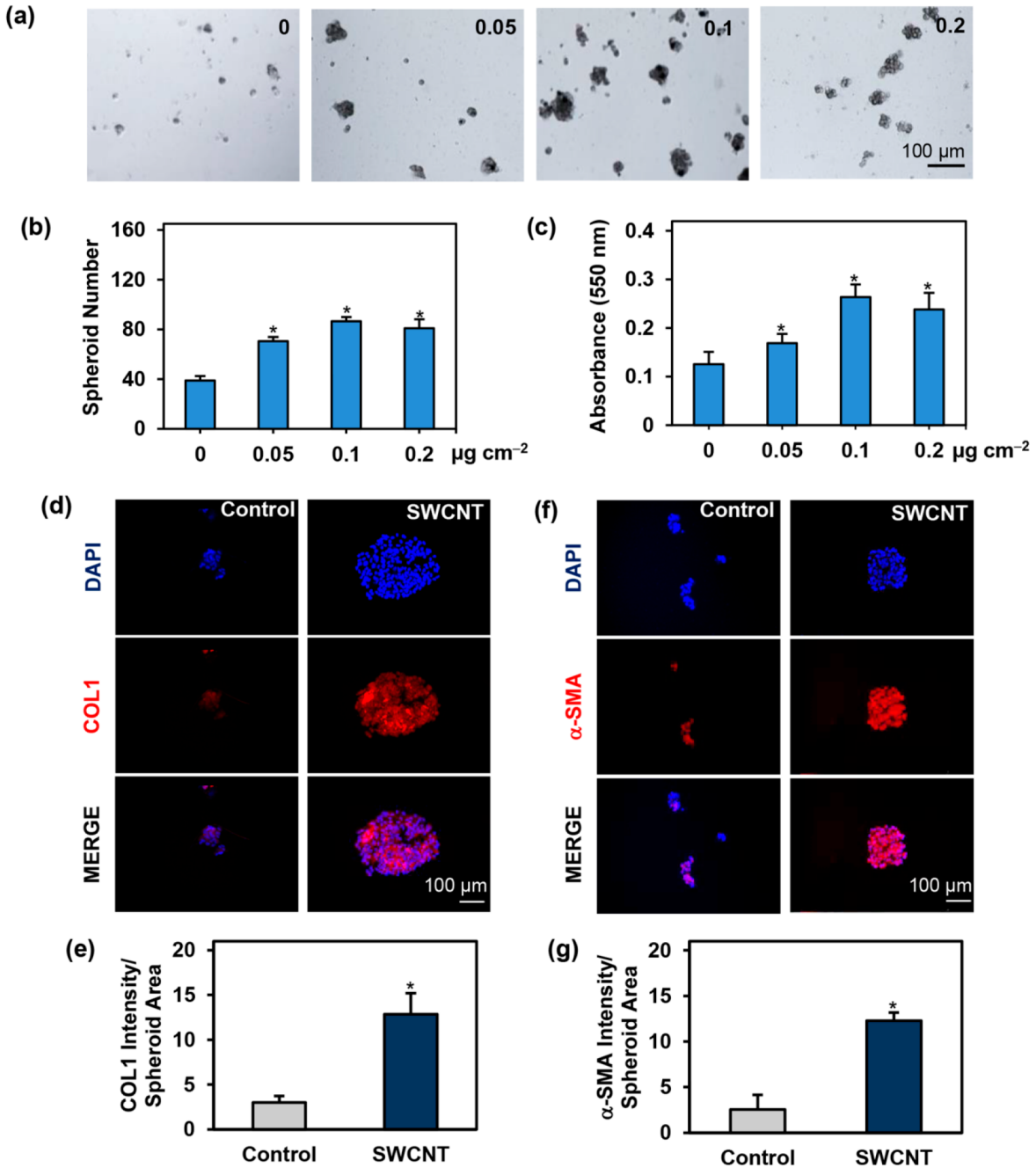

Figure 4. Induction of stem cell properties by SWCNTs in primary human lung fibroblasts. Cells were grown under nonadherent conditions with SWCNTs (0−0.2 μg cm^{-2} or 0−0.95 μg mL^{-1}). (a) Representative images of 3D spheroids at 14 days postplating. The scale bar is 100 μm. 100× magnification. (b) Quantification of spheroid numbers. (c) Detection of collagen production in the cell culture medium of spheroids by Sircol assay. (d−g) Quantification and representative immunofluorescence images of spheroids showing type 1 collagen, α-SMA, and nucleus staining. The scale bar is 100 μm. 200× magnification. Data presented as mean ± SD (n = 3), *p < 0.05 versus control cells.

myocardial infarction, the silencing of ABCG2 resulted in a substantial reduction of myofibroblast density in peri-infarction areas,[59] suggesting the role of stem cells in fibrosis remodeling.

To further investigate the molecular mechanisms of stem cell induction by SWCNTs and its role in fibrogenesis, we evaluated key transcription factors known to be significant regulators of stem cell functions, including OCT4, NANOG, and SOX2.[65,66] NHLFs were treated with noncytotoxic doses of SWCNTs and analyzed for these transcription factors by Western blotting. Figure 6a,b shows that OCT4 and NANOG were weakly expressed in NHLFs and were relatively unaffected by the SWCNT treatment. In contrast, SOX2 was substantially expressed in these cells and was significantly upregulated in the SWCNT-treated cells. Immunofluorescence studies further showed that SOX2 was upregulated in spheroid-forming cells from SWCNT-treated fibroblasts than untreated controls (Figure 6c,d). Interestingly, these cells also expressed a high level of COL1, suggesting their possible causal relationship. To investigate this possibility, NHLFs were treated with SWCNTs and analyzed for SOX2 and COL1 coexpression by flow cytometry. Figure 6e shows that the majority (57%) of NHLFs coexpressed SOX2 and COL1, and

https://dx.doi.org/10.1021/acsbiomaterials.0c00887
ACS Biomater. Sci. Eng. 2020, 6, 5290−5304

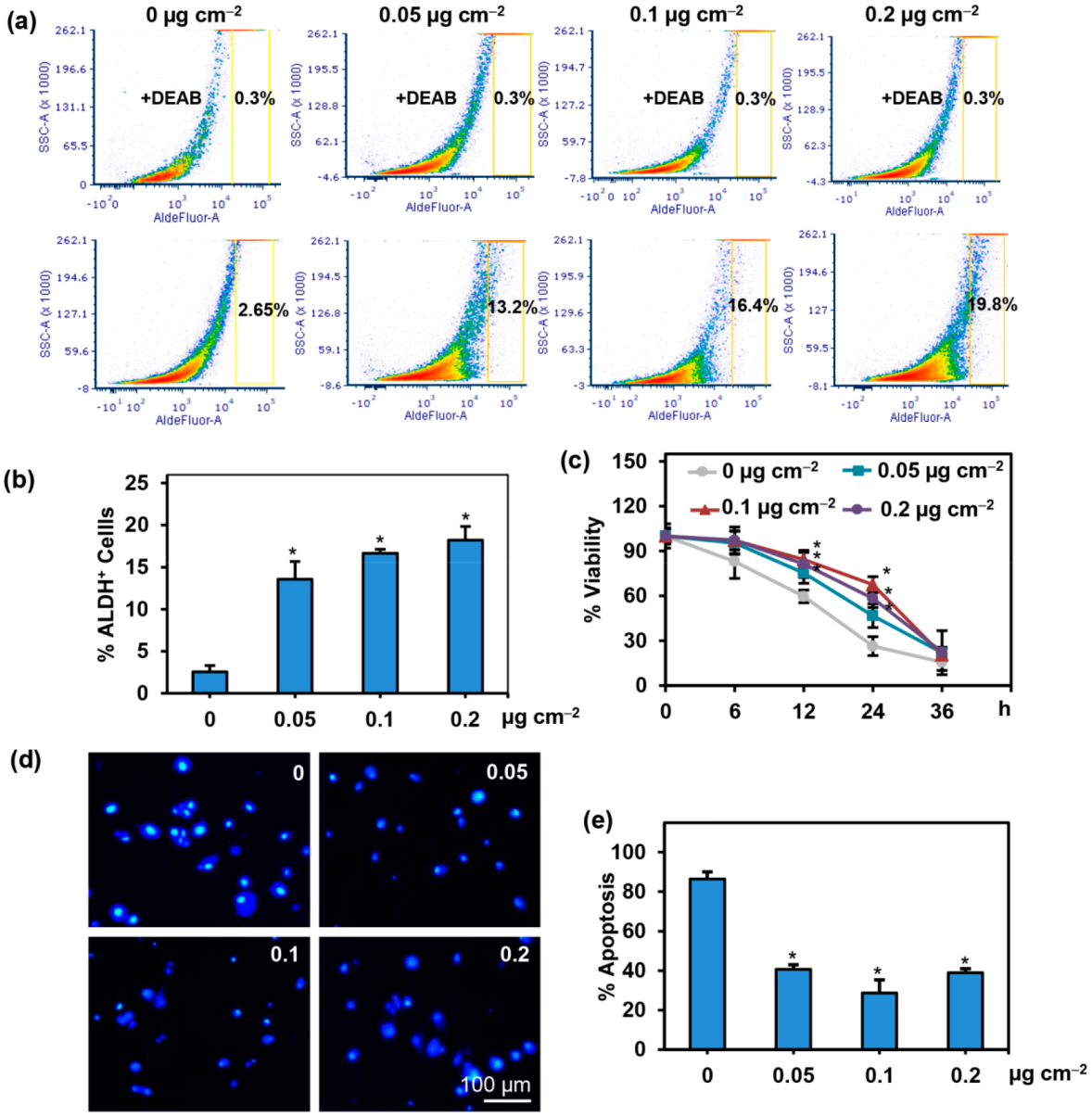

Figure 5. Activation of aldehyde dehydrogenase (ALDH) and induction of anoikis resistance by SWCNTS in primary human lung fibroblasts. Cells were treated with SWCNTs (0−0.2 μg cm^{-2} or 0−0.95 μg mL^{-1}) for 48 h and ALDH activity was evaluated by flow cytometry using Aldefluor assay. (a) Representative FACS plots of ALDH activity in SWCNT-treated cells with or without the ALDH inhibitor DEAB, which was used as an internal control for baseline ALDH activity measurements. (b) Quantification of ALDH activity. (c) After exposure to SWCNTs for 48 h, cells were replated, incubated under nonadherent conditions for 36 h, and analyzed for anoikis or detachment-induced cell death. Viability after detachment was determined by MTS assay. (d) Representative images of Hoechst 33342 stained cells. Apoptotic nuclei are brightly fluorescent due to DNA condensation, a characteristic of apoptotic cells. The scale bar is 100 μm. 100× magnification. (e) Percentage of apoptotic cells after detachment determined by Hoechst 33342 assay. Data presented as mean ± SD (n = 3), *p < 0.05 versus control cells.

this number substantially increased (~80%) when the cells were treated with SWCNTs. Pearson correlation analysis of SOX2 and COL1 expression based on immunofluorescence intensities from flow cytometry experiments revealed a positive correlation between SOX2 and COL1 in SWCNT-treated cells (Figure 6f). Such correlation was also observed in vivo in SWCNT-treated mice, where colocalization and concurrent upregulation of SOX2 and COL1 were observed in the lungs of SWCNT-treated mice (Figure 6g,h). This finding strongly supports mechanistic link and potential causal relationship between SOX2 and COL1, which was further investigated in subsequent studies below. It should be noted that while SOX2 and fibrosis correlation has been observed in various tissues induced by various agents,[67,68] their direct causal relationship has yet to be demonstrated.

3.5. SOX2 Transcriptionally Regulates COL1 in NHLFs. Based on concurrent expression and upregulation of SOX2 and COL1 in SWCNT-treated cells and tissues (Figure 6c-h) and the established role of SOX2 as a transcription factor, we tested whether SOX2 could be a direct transcriptional regulator of COL1. NHLFs were treated with short-hairpin RNA against SOX2 (shSOX2) or control shRNA (shCON) via lentivirus-mediated transduction, and their effect on COL1 expression was determined by Western blotting and immunofluorescence staining. Figure 7a,b (and Figure S3) shows that SOX2 expression was downregulated in shSOX2

https://dx.doi.org/10.1021/acsbiomaterials.0c00887
ACS Biomater. Sci. Eng. 2020, 6, 5290−5304

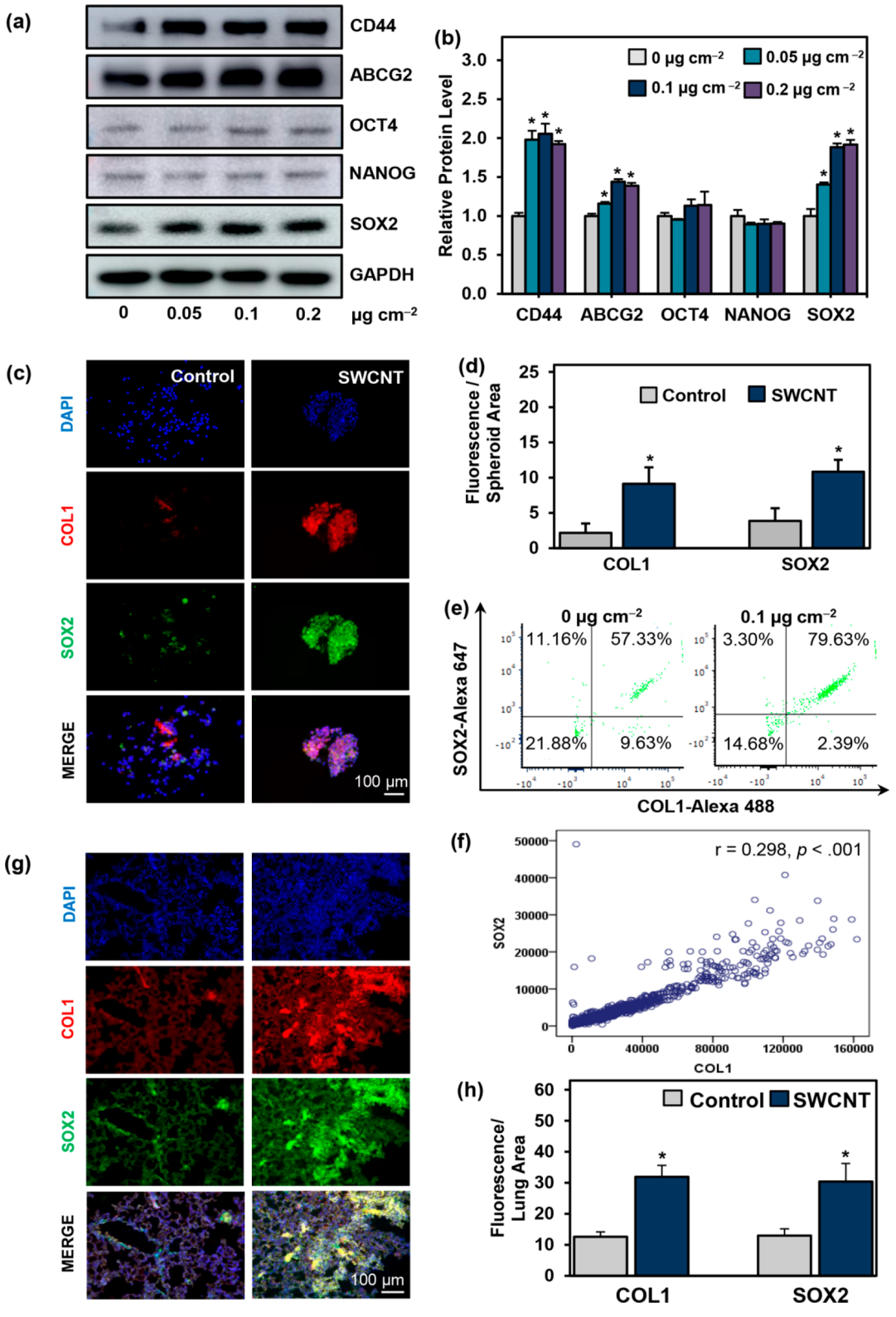

Figure 6. Induction of stem cell markers and self-renewal transcription factors by SWCNTs in human lung fibroblasts and mouse lung tissues. NHLFs were exposed to SWCNTs (0−0.2 μg cm^{-2} or 0−0.95 μg mL^{-1}) for 48 h. (a,b) Immunoblot analysis and quantification of CD44, ABCG2, OCT4, NANOG, and SOX2 in the treated cells. (c,d) Representative immunofluorescence images of spheroids and quantification of type 1 collagen (red) and SOX2 (green) in the spheroids. The scale bar is 100 μm. 200× magnification. (e) Flow cytometric analysis of SOX2 and COL1 expression in control and SWCNT-treated fibroblasts. The cells in each quadrant are indicated on the plots. (f) Correlation analysis of SOX2 and COL1 expression in SWCNT-treated cells. (g,h) Representative immunofluorescence images of SWCNT-treated mouse lungs and quantification of type 1 collagen (red) and SOX2 (green) at 56 days postexposure. The scale bar is 100 μm. 200× magnification. Data presented as mean ± SD (n = 3), *p < 0.05 versus control cells.

https://dx.doi.org/10.1021/acsbiomaterials.0c00887
ACS Biomater. Sci. Eng. 2020, 6, 5290−5304

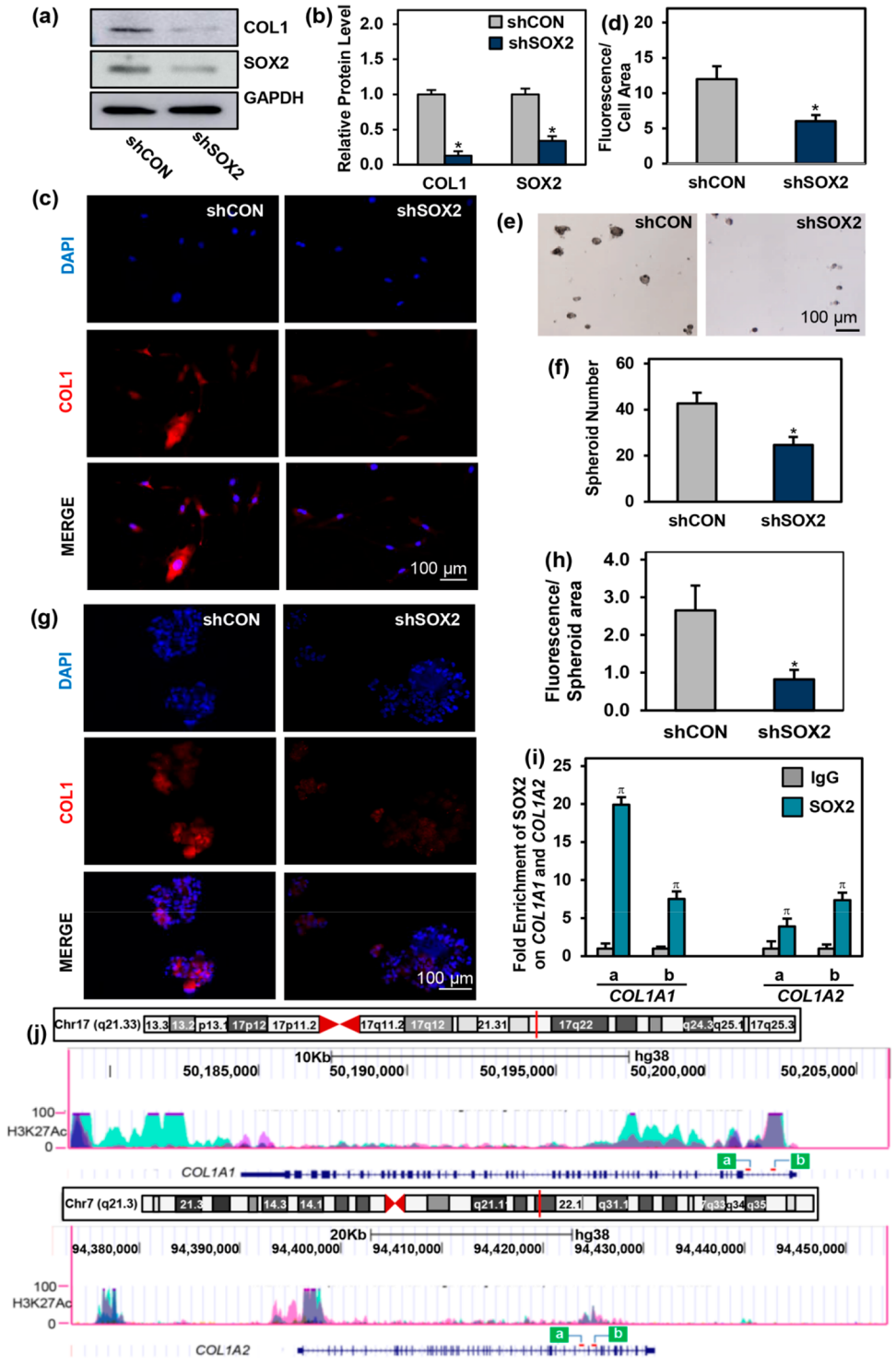

Figure 7. Suppression of type 1 collagen expression and stem cell properties by SOX2 knockdown in primary human lung fibroblasts. The knockdown of SOX2 was carried out using short-hairpin RNA (shRNA) lentiviral particles. (a,b) Western blot analysis and quantification of type 1 collagen and SOX2 in shRNA control (shCON) and SOX2 knockdown (shSOX2) cells. (c,d) Representative immunofluorescence images and quantification of type 1 collagen (red) staining in shCON and shSOX2 cells. The scale bar is 100 μm. 100× magnification. shCON and shSOX2 cells were grown under nonadherent conditions for 14 days. (e,f) Representative images of 3D spheroids and quantification of spheroid numbers in shCON and shSOX2 cells at day 14 postplating. The scale bar is 100 μm. 100× magnification. (g,h) Representative immunofluorescence images of spheroids formed by shCON and shSOX2 cells and quantification of type 1 collagen (red) staining in the spheroids. The scale bar is 100 μm. 200× magnification. Chromatin immunoprecipitation assay was performed in NHLFs to estimate the enrichment of SOX2 on *COL1A1* and *COL1A2*. (i) After normalization of the input, fold enrichment was assessed and compared to the immunoglobulin G as a negative control (IgG; set as 1). (j) Screenshot location of SOX2 on *COL1A1* and *COL1A2* on its chromosome as indicated by a red vertical line, *COL1A1* and *COL1A2* gene structures with H3K27Ac clusters uploaded in the University of California, Santa Cruz genome browser and binding sites of SOX2 on *COL1A1* and *COL1A2* in our study as indicated by a red horizontal line. Data presented as mean ± SD (n = 3), *p < 0.05 versus shCON cells. $^{\pi}p$ <0.05 versus IgG.

https://dx.doi.org/10.1021/acsbiomaterials.0c00887
ACS Biomater. Sci. Eng. 2020, 6, 5290−5304

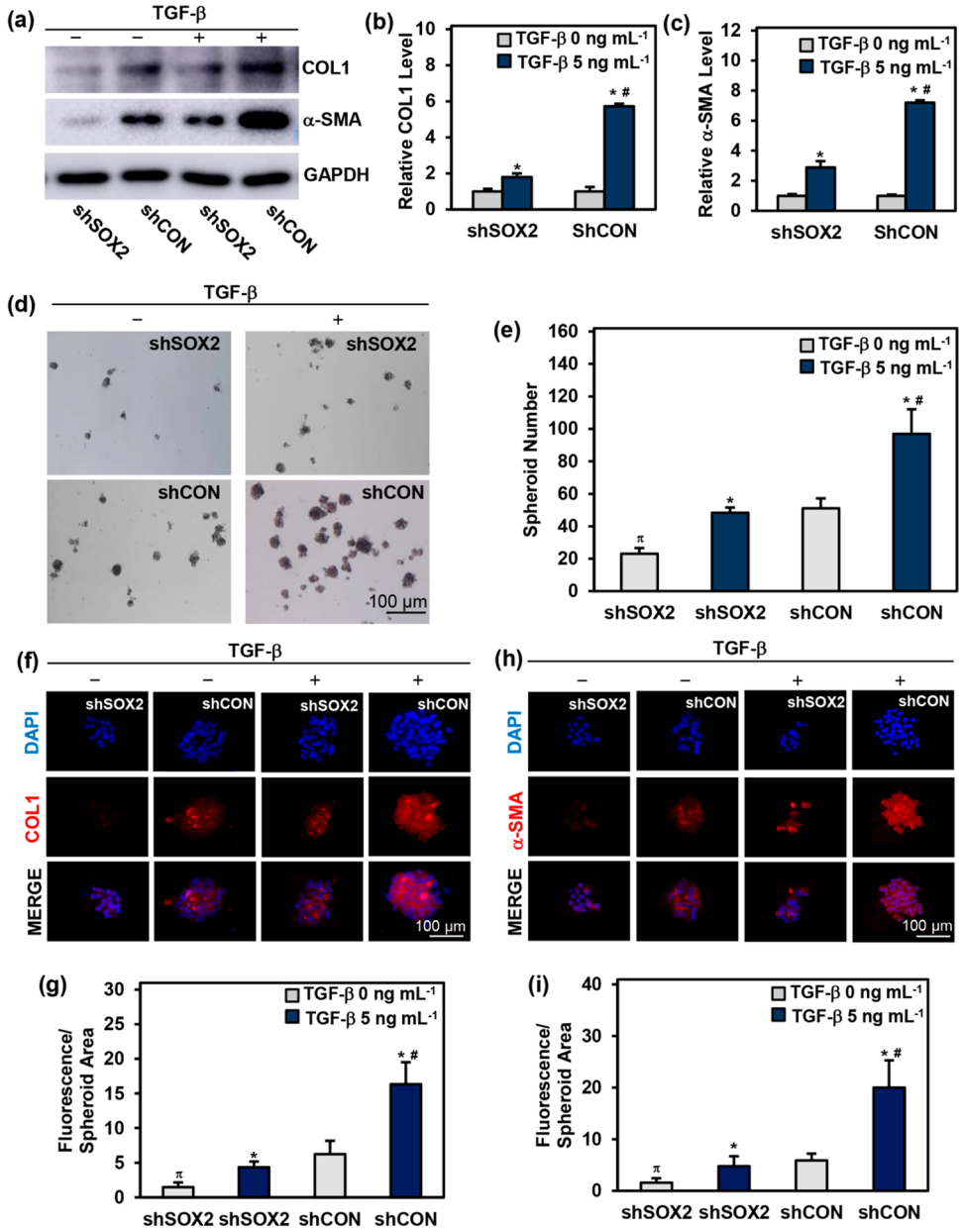

Figure 8. Inhibition of TGF-β-induced fibrogenic responses by SOX2 knockdown in primary human lung fibroblasts. shRNA control (shCON) and SOX2 knockdown (shSOX2) cells were treated with TGF-β (5 ng mL^{-1}) for 48 h. (a–c) Western blot analysis and quantification of COL1 and α-SMA in shCON and shSOX2 cells. shCON and shSOX2 cells were cultured in nonadherent conditions with or without TGF-β for 14 days. (d,e) Representative images of 3D spheroids after 14 days of plating and quantification of spheroid numbers. The scale bar is 100 μm. 100× magnification. (f–i) Representative images of spheroids at day 14 and quantification of COL1 (red) and α-SMA (red). The scale bar is 100 μm. 200× magnification. Data presented as mean ± SD (n = 3), *p < 0.05 versus untreated shCON, or untreated shSOX2 cells. $^{\#}p$ < 0.05 versus TGF-β-treated shSOX2 cells.

cells as compared to shCON cells. shSOX2 cells also expressed a significantly lower level of COL1 relative to shCON cells, as shown by immunofluorescence (Figure 7c,d) and immunoblot results (Figure 7a,b). Sphere formation studies further showed that shSOX2 cells exhibited substantially lower sphere-forming activity than the control cells (Figure 7e,f) and that COL1 expression in these cells followed a similar pattern (Figure 7g,h). These results indicate that SOX2 is required for both stem cell phenotype and COL1 expression in NHLFs.

COL1 is a triple-helical structure comprising of two α1 and one α2 chains that are produced from *COL1A1* and *COL1A2*, respectively.[69] To test whether they are a direct transcriptional target of SOX2, we performed chromatin immunoprecipitation (ChIP) assay to determine SOX2-binding sites on *COL1A1* and *COL1A2* in NHLFs. Relative fold enrichment of SOX2 on *COL1A1* and *COL1A2* was determined using immunoglobulin G as a negative control. The result of this study (Figure 7i) and additional genome analysis of *COL1A1* and *COL1A2* gene structures (Figure 7j) indicated significant SOX2 binding on *COL1A1* and *COL1A2* in NHLFs. This result supports the earlier gene knockdown finding and indicates that SOX2 regulation of COL1 is likely due to transcriptional activation of *COL1A1* and *COL1A2*.

3.6. SOX2 Regulates TGF-β Fibrogenesis. Since SOX2 appears to be upregulated in various fibrotic tissues and by various agents,[39,40] we tested whether SOX2 could be a general

https://dx.doi.org/10.1021/acsbiomaterials.0c00887
ACS Biomater. Sci. Eng. 2020, 6, 5290–5304

regulator of fibrosis and not only SWCNT-induced fibrosis. To test this, we treated NHLFs with TGF-β, which is a known fibrogenic mediator induced by various fibrotic agents, including CNTs[33,70] and its effects on COL1 and α-SMA expression were determined in SOX2 knockdown and control cells. Figure 8a−c shows that treatment of the cells with TGF-β significantly upregulated COL1 and α-SMA expression in both shCON and shSOX2 cells, but the effect was much more pronounced in the shCON cells, indicating the requirement of SOX2 in the fibrotic response. TGF-β treatment also induced sphere formation in shCON cells and shSOX2 cells, with the effect being less pronounced in the shSOX2 cells (Figure 8d,e), supporting the role of SOX2 in the fibrotic response. The reduced ability of TGF-β to induce sphere formation in shSOX2 cells also indicates the requirement of SOX2 in TGF-β-induced FSCs. These results were substantiated by immunofluorescence staining studies showing high COL1 and α-SMA expression in the spheroids of TGF-β-treated shCON cells, which were weakly expressed in TGF-β-treated shSOX2 cells (Figure 8f−i). Together, these results indicate the functional role of SOX2 as a master regulator of fibrogenic signaling induced by TGF-β and SWCNTs and suggest this transcription factor as an early biomarker of nanomaterial-induced fibrotic diseases.

4. CONCLUSIONS

In summary, we demonstrated the induction of stem cell properties of NHLFs by SWCNTs as indicated by spheroid formation, anoikis/apoptosis resistance, and stem cell markers expression. Such induction is associated with the fibrogenic activities of SWCNTs since inhibition of fibroblast stem cells by SOX2 knockdown abrogated the collagen- and α-SMA inducing effects of SWCNTs. SOX2 was found to be a key regulator of fibrogenesis induced by both SWCNTs and TGF-β, suggesting its broader role as a master regulator of fibrogenesis. Mechanistic studies revealed SOX2 regulation of collagen expression via transcriptional activation of *COL1A1* and *COL1A2*. This novel finding may have broad implications on the fibrogenic mechanisms of nanomaterials and the development of predictive early biomarkers for nanomaterial-induced fibrosis. The results of this study also support the use of FSCs as an alternate in vitro model for fibrogenicity testing of nanomaterials, i.e., through 3D sphere formation assay, based on their ability to drive and sustain fibrogenesis.

■ ASSOCIATED CONTENT

Supporting Information

The Supporting Information is available free of charge at https://pubs.acs.org/doi/10.1021/acsbiomaterials.0c00887.

Table S1, hydrodynamic diameter and zeta potential of SWCNT 0.1 mg mL-1 in sterile water and 0.5% BSA in dPBS; Table S2, carbon nanotube (CNT) doses for in vitro studies; Table S3, primer oligonucleotide sequences used for RT-qPCR studies; Figure S1, EDS spectra of pristine SWCNTs; Figure S2, the effect of SWCNTs on TGF-β and matrix metalloproteinases (MMPs) expressions; Figure S3, expression of SOX2 in shCON and shSOX2 cells; Figure S4, the effect of SOX2 knockdown on fibronectin 1 (FN1) expression (PDF)

■ AUTHOR INFORMATION

Corresponding Author

Yon Rojanasakul − *Department of Pharmaceutical Sciences and WVU Cancer Institute, West Virginia University, Morgantown, West Virginia 26506, United States*; Phone: 304-293-1476; Email: yrojan@hsc.wvu.edu; Fax: 304-293 2576

Authors

Chayanin Kiratipaiboon − *Department of Pharmaceutical Sciences, West Virginia University, Morgantown, West Virginia 26506, United States*; orcid.org/0000-0002-6901-131X

Maria Voronkova − *WVU Cancer Institute, West Virginia University, Morgantown, West Virginia 26506, United States*

Rajib Ghosh − *Department of Pharmaceutical Sciences, West Virginia University, Morgantown, West Virginia 26506, United States*

Liying W. Rojanasakul − *Health Effects Laboratory Division, National Institute for Occupational Safety and Health, Morgantown, West Virginia 26505, United States*

Cerasela Zoica Dinu − *Department of Chemical and Biomedical Engineering, Benjamin M. Statler College of Engineering and Mineral Resources, West Virginia University, Morgantown, West Virginia 26506, United States*; orcid.org/0000-0002-6474-6771

Yi Charlie Chen − *College of Health Science, Technology and Mathematics, Alderson Broaddus University, Philippi, West Virginia 26416, United States*

Complete contact information is available at: https://pubs.acs.org/10.1021/acsbiomaterials.0c00887

Author Contributions

C.K. carried out most of the experiments, analyzed data, and drafted the manuscript. M.V. assisted with chromatin immunoprecipitation experiments and tissue collection. R.G. participated in animal experiments, tissue collection and manuscript preparation. L.W.R. assisted in electron microscopy and animal studies. C.Z.D. assisted in physicochemical characterization of SWCNTs and data analysis. Y.C.C. assisted in molecular analyses and interpretation of data. Y.R. coordinated the whole study and participated in all aspects of the study. All authors approved the final version of the manuscript.

Notes

The authors declare no competing financial interest.

■ ACKNOWLEDGMENTS

This work was supported by the National Institutes of Health (NIH) (R01-ES022968 and R01-EB018857). Flow cytometry experiments were performed in the WVU Flow Cytometry and Single Cell Analysis Core Facility, which is supported by the NIH equipment Grant S10OD16165 and the NIH Institutional Development Award (IDeA) through Grants P30GM103488 (CoBRE) and P20GM103434 (INBRE).

■ REFERENCES

(1) McWilliams, A. Global Markets for Nanocomposites, Nanoparticles, Nanoclays, and Nanotubes. *NAN021G*. **2017**.

(2) Jafari, S. Engineering applications of carbon nanotubes. *Carbon Nanotube-Reinforced Polymers*; Elsevier: Amsterdam, 2018; pp 25−40.

(3) Shahidi, S.; Moazzenchi, B. Carbon nanotube and its applications in textile industry−A review. *J. Text. Inst.* **2018**, *109*, 1653−66.

(4) Rao, R.; Pint, C. L.; Islam, A. E.; Weatherup, R. S.; Hofmann, S.; Meshot, E. R.; Wu, F.; Zhou, C.; Dee, N.; Amama, P. B.; Carpena-Nunez, J.; Shi, W.; Plata, D. L.; Penev, E. S.; Yakobson, B. I.; Balbuena, P. B.; Bichara, C.; Futaba, D. N.; Noda, S.; Shin, H.; Kim, K. S.; Simard, B.; Mirri, F.; Pasquali, M.; Fornasiero, F.; Kauppinen, E. I.; Arnold, M.; Cola, B. A.; Nikolaev, P.; Arepalli, S.; Cheng, H.-M.; Zakharov, D. N.; Stach, E. A.; Zhang, J.; Wei, F.; Terrones, M.; Geohegan, D. B.; Maruyama, B.; Maruyama, S.; Li, Y.; Adams, W. W.; Hart, A. J. Carbon nanotubes and related nanomaterials: critical advances and challenges for synthesis toward mainstream commercial applications. *ACS Nano* **2018**, *12*, 11756−84.

(5) Neelgund, G. M.; Oki, A. Advancement in photothermal effect of carbon nanotubes by grafting of poly (amidoamine) and deposition of CdS nanocrystallites. *Ind. Eng. Chem. Res.* **2018**, *57*, 7826−33.

(6) Zhu, Y.; Sun, Q.; Liu, Y.; Ma, T.; Su, L.; Liu, S.; Shi, X.; Han, D.; Liang, F. Decorating gold nanostars with multiwalled carbon nanotubes for photothermal therapy. *R. Soc. Open Sci.* **2018**, *5*, 180159.

(7) Yudasaka, M.; Yomogida, Y.; Zhang, M.; Tanaka, T.; Nakahara, M.; Kobayashi, N.; Okamatsu-Ogura, Y.; Machida, K.; Ishihara, K.; Saeki, K.; Kataura, H. Near-infrared photoluminescent carbon nanotubes for imaging of brown fat. *Sci. Rep.* **2017**, *7*, 44760.

(8) Huth, K.; Glaeske, M.; Achazi, K.; Gordeev, G.; Kumar, S.; Arenal, R.; Sharma, S. K.; Adeli, M.; Setaro, A.; Reich, S.; Haag, R. Fluorescent Polymer—Single-Walled Carbon Nanotube Complexes with Charged and Noncharged Dendronized Perylene Bisimides for Bioimaging Studies. *Small* **2018**, *14*, 1800796.

(9) Donaldson, K.; Murphy, F. A.; Duffin, R.; Poland, C. A. Asbestos, carbon nanotubes and the pleural mesothelium: a review of the hypothesis regarding the role of long fibre retention in the parietal pleura, inflammation and mesothelioma. *Part. Fibre Toxicol.* **2010**, *7*, 5.

(10) Dong, J.; Ma, Q. Advances in mechanisms and signaling pathways of carbon nanotube toxicity. *Nanotoxicology* **2015**, *9*, 658−76.

(11) Kobayashi, N.; Izumi, H.; Morimoto, Y. Review of toxicity studies of carbon nanotubes. *J. Occup. Health* **2017**, *59*, 394.

(12) Mercer, R. R.; Scabilloni, J.; Wang, L.; Kisin, E.; Murray, A. R.; Schwegler-Berry, D.; Shvedova, A. A.; Castranova, V. Alteration of deposition pattern and pulmonary response as a result of improved dispersion of aspirated single-walled carbon nanotubes in a mouse model. *Am. J. Physiol Lung Cell Mol. Physiol.* **2008**, *294*, L87−97.

(13) Konduru, N. V.; Tyurina, Y. Y.; Feng, W.; Basova, L. V.; Belikova, N. A.; Bayir, H.; Clark, K.; Rubin, M.; Stolz, D.; Vallhov, H.; Scheynius, A.; Witasp, E.; Fadeel, B.; Kichambare, P. D.; Star, A.; Kisin, E. R.; Murray, A. R.; Shvedova, A. A.; Kagan, V. E. Phosphatidylserine targets single-walled carbon nanotubes to professional phagocytes in vitro and in vivo. *PLoS One* **2009**, *4*, No. e4398.

(14) Mercer, R. R.; Hubbs, A. F.; Scabilloni, J. F.; Wang, L.; Battelli, L. A.; Schwegler-Berry, D.; Castranova, V.; Porter, D. W. Distribution and persistence of pleural penetrations by multi-walled carbon nanotubes. *Part. Fibre Toxicol.* **2010**, *7*, 28.

(15) Oberdörster, G.; Castranova, V.; Asgharian, B.; Sayre, P. Inhalation exposure to carbon nanotubes (CNT) and carbon nanofibers (CNF): Methodology and dosimetry. *J. Toxicol. Environ. Health, Part B* **2015**, *18*, 121−212.

(16) Shinohara, N.; Nakazato, T.; Ohkawa, K.; Tamura, M.; Kobayashi, N.; Morimoto, Y.; Oyabu, T.; Myojo, T.; Shimada, M.; Yamamoto, K.; Tao, H.; Ema, M.; Naya, M.; Nakanishi, J. Long-term retention of pristine multi-walled carbon nanotubes in rat lungs after intratracheal instillation. *J. Appl. Toxicol.* **2016**, *36*, 501−9.

(17) Hesterberg, T. W.; Chase, G.; Axten, C.; Miller, W. C.; Musselman, R. P.; Kamstrup, O.; Hadley, J.; Morscheidt, C.; Bernstein, D. M.; Thevenaz, P. Biopersistence of synthetic vitreous fibers and amosite asbestos in the rat lung following inhalation. *Toxicol. Appl. Pharmacol.* **1998**, *151*, 262−75.

(18) Bernstein, D. M.; Riego Sintes, J. M.; Ersboell, B. K.; Kunert, J. Biopersistence of synthetic mineral fibers as a predictor of chronic inhalation toxicity in rats. *Inhalation Toxicol.* **2001**, *13*, 823−849.

(19) Rydman, E. M.; Ilves, M.; Vanhala, E.; Vippola, M.; Lehto, M.; Kinaret, P. A.; Pylkkanen, L.; Happo, M.; Hirvonen, M. R.; Greco, D.; Savolainen, K.; Wolff, H.; Alenius, H. A Single Aspiration of Rod-like Carbon Nanotubes Induces Asbestos-like Pulmonary Inflammation Mediated in Part by the IL-1 Receptor. *Toxicol. Sci.* **2015**, *147*, 140−55.

(20) Cartwright, M. M.; Schmuck, S. C.; Corredor, C.; Wang, B.; Scoville, D. K.; Chisholm, C. R.; Wilkerson, H.-W.; Afsharinejad, Z.; Bammler, T. K.; Posner, J. D.; Shutthanandan, V.; Baer, D. R.; Mitra, S.; Altemeier, W. A.; Kavanagh, T. J. The pulmonary inflammatory response to multiwalled carbon nanotubes is influenced by gender and glutathione synthesis. *Redox Biol.* **2016**, *9*, 264−275.

(21) Poulsen, S. S.; Jackson, P.; Kling, K.; Knudsen, K. B.; Skaug, V.; Kyjovska, Z. O.; Thomsen, B. L.; Clausen, P. A.; Atluri, R.; Berthing, T.; Bengtson, S.; Wolff, H.; Jensen, K. A.; Wallin, H.; Vogel, U. Multi-walled carbon nanotube physicochemical properties predict pulmonary inflammation and genotoxicity. *Nanotoxicology* **2016**, *10*, 1263−75.

(22) Huizar, I.; Malur, A.; Midgette, Y. A.; Kukoly, C.; Chen, P.; Ke, P. C.; Podila, R.; Rao, A. M.; Wingard, C. J.; Dobbs, L.; Barna, B. P.; Kavuru, M. S.; Thomassen, M. J. Novel murine model of chronic granulomatous lung inflammation elicited by carbon nanotubes. *Am. J. Respir. Cell Mol. Biol.* **2011**, *45*, 858−66.

(23) Sturm, R. Clearance of carbon nanotubes in the human respiratory tract-a theoretical approach. *Ann. Transl Med.* **2014**, *2*, 46.

(24) Honda, K.; Naya, M.; Takehara, H.; Kataura, H.; Fujita, K.; Ema, M. A 104-week pulmonary toxicity assessment of long and short single-wall carbon nanotubes after a single intratracheal instillation in rats. *Inhalation Toxicol.* **2017**, *29*, 471−82.

(25) Lam, C.-W. Pulmonary toxicity of single-wall carbon nanotubes in mice 7 and 90 days after intratracheal instillation. *Toxicol. Sci.* **2003**, *77*, 126−34.

(26) Shvedova, A. A.; Kisin, E. R.; Mercer, R.; Murray, A. R.; Johnson, V. J.; Potapovich, A. I.; Tyurina, Y. Y.; Gorelik, O.; Arepalli, S.; Schwegler-Berry, D.; Hubbs, A. F.; Antonini, J.; Evans, D. E.; Ku, B. K.; Ramsey, D.; Maynard, A.; Kagan, V. E.; Castranova, V.; Baron, P. Unusual inflammatory and fibrogenic pulmonary responses to single-walled carbon nanotubes in mice. *Am. J. Physiol Lung Cell Mol. Physiol.* **2005**, *289*, L698−708.

(27) Mercer, R. R.; Hubbs, A. F.; Scabilloni, J. F.; Wang, L.; Battelli, L. A.; Friend, S.; Castranova, V.; Porter, D. W. Pulmonary fibrotic response to aspiration of multi-walled carbon nanotubes. *Part. Fibre Toxicol.* **2011**, *8*, 21.

(28) Shvedova, A. A.; Kisin, E.; Murray, A. R.; Johnson, V. J.; Gorelik, O.; Arepalli, S.; Hubbs, A. F.; Mercer, R. R.; Keohavong, P.; Sussman, N.; Jin, J.; Yin, J.; Stone, S.; Chen, B. T.; Deye, G.; Maynard, A.; Castranova, V.; Baron, P. A.; Kagan, V. E. Inhalation vs. aspiration of single-walled carbon nanotubes in C57BL/6 mice: inflammation, fibrosis, oxidative stress, and mutagenesis. *Am. J. Physiol Lung Cell Mol. Physiol.* **2008**, *295*, L552−65.

(29) Park, E. J.; Roh, J.; Kim, S. N.; Kang, M. S.; Han, Y. A.; Kim, Y.; Hong, J. T.; Choi, K. A single intratracheal instillation of single-walled carbon nanotubes induced early lung fibrosis and subchronic tissue damage in mice. *Arch. Toxicol.* **2011**, *85*, 1121−31.

(30) Murray, A. R.; Kisin, E. R.; Tkach, A. V.; Yanamala, N.; Mercer, R.; Young, S.-H.; Fadeel, B.; Kagan, V. E.; Shvedova, A. A. Factoring-in agglomeration of carbon nanotubes and nanofibers for better prediction of their toxicity versus asbestos. *Part. Fibre Toxicol.* **2012**, *9*, 10.

(31) Wang, L.; Castranova, V.; Mishra, A.; Chen, B.; Mercer, R. R.; Schwegler-Berry, D.; Rojanasakul, Y. Dispersion of single-walled carbon nanotubes by a natural lung surfactant for pulmonary in vitro and in vivo toxicity studies. *Part. Fibre Toxicol.* **2010**, *7*, 31.

(32) Luanpitpong, S.; Wang, L.; Manke, A.; Martin, K. H.; Ammer, A. G.; Castranova, V.; Yang, Y.; Rojansakul, Y. Induction of stemlike

https://dx.doi.org/10.1021/acsbiomaterials.0c00887
ACS Biomater. Sci. Eng. 2020, 6, 5290−5304

cells with fibrogenic properties by carbon nanotubes and its role in fibrogenesis. *Nano Lett.* **2014**, *14*, 3110−6.
(33) Mishra, A.; Stueckle, T. A.; Mercer, R. R.; Derk, R.; Rojanasakul, Y.; Castranova, V.; Wang, L. Identification of TGF-β receptor-1 as a key regulator of carbon nanotube-induced fibrogenesis. *Am. J. Physiol Lung Cell Mol. Physiol.* **2015**, *309*, L821−L33.
(34) Yazdani, S.; Bansal, R.; Prakash, J. Drug targeting to myofibroblasts: Implications for fibrosis and cancer. *Adv. Drug Delivery Rev.* **2017**, *121*, 101−16.
(35) Sharma, M.; Nikota, J.; Halappanavar, S.; Castranova, V.; Rothen-Rutishauser, B.; Clippinger, A. J. Predicting pulmonary fibrosis in humans after exposure to multi-walled carbon nanotubes (MWCNTs). *Arch. Toxicol.* **2016**, *90*, 1605−22.
(36) Rao, B.; Malathi, N.; Narashiman, S.; Rajan, S. T. Evaluation of myofibroblasts by expression of alpha smooth muscle actin: a marker in fibrosis, dysplasia and carcinoma. *J. Clin Diagn Res.* **2014**, *8*, ZC14.
(37) Jun, J.-I.; Lau, L. F. Resolution of organ fibrosis. *J. Clin. Invest.* **2018**, *128*, 97−107.
(38) Distler, J. H.; Györfi, A.-H.; Ramanujam, M.; Whitfield, M. L.; Königshoff, M.; Lafyatis, R. Shared and distinct mechanisms of fibrosis. *Nat. Rev. Rheumatol.* **2019**, *15*, 705.
(39) Sakurai, T.; Kudo, M.; Umemura, A.; He, G.; Elsharkawy, A. M.; Seki, E.; Karin, M. p38alpha inhibits liver fibrogenesis and consequent hepatocarcinogenesis by curtailing accumulation of reactive oxygen species. *Cancer Res.* **2013**, *73*, 215−24.
(40) Liu, S.; Herault, Y.; Pavlovic, G.; Leask, A. Skin progenitor cells contribute to bleomycin-induced skin fibrosis. *Arthritis Rheumatol.* **2014**, *66*, 707−13.
(41) Xia, H.; Bodempudi, V.; Benyumov, A.; Hergert, P.; Tank, D.; Herrera, J.; Braziunas, J.; Larsson, O.; Parker, M.; Rossi, D.; Smith, K.; Peterson, M.; Limper, A.; Jessurun, J.; Connett, J.; Ingbar, D.; Phan, S.; Bitterman, P. B.; Henke, C. A. Identification of a cell-of-origin for fibroblasts comprising the fibrotic reticulum in idiopathic pulmonary fibrosis. *Am. J. Pathol.* **2014**, *184*, 1369−83.
(42) Ambade, A.; Satishchandran, A.; Szabo, G. Alcoholic hepatitis accelerates early hepatobiliary cancer by increasing stemness and miR-122-mediated HIF-1alpha activation. *Sci. Rep.* **2016**, *6*, 21340.
(43) Grant, C.; Chudakova, D. A.; Itinteang, T.; Chibnall, A. M.; Brasch, H. D.; Davis, P. F.; Tan, S. T. Expression of embryonic stem cell markers in keloid-associated lymphoid tissue. *J. Clin. Pathol.* **2016**, *69*, 643−6.
(44) He, X.; Kiratipaiboon, C.; Porter, D. W.; Rojanasakul, L. W.; Dinu, C. Z.; Wang, K.; Yang, Y.; Rojanasakul, Y. Predicting Nanotube Fibrogenicity through Stem Cell-Mediated Fibroblast Focus and Spheroid Formation. *Nano Lett.* **2018**, *18*, 6500−8.
(45) Cha, S. I.; Groshong, S. D.; Frankel, S. K.; Edelman, B. L.; Cosgrove, G. P.; Terry-Powers, J. L.; Remigio, L. K.; Curran-Everett, D.; Brown, K. K.; Cool, C. D.; Riches, D. W. Compartmentalized expression of c-FLIP in lung tissues of patients with idiopathic pulmonary fibrosis. *Am. J. Respir. Cell Mol. Biol.* **2010**, *42*, 140−8.
(46) Harada, T.; Watanabe, K.; Nabeshima, K.; Hamasaki, M.; Iwasaki, H. Prognostic significance of fibroblastic foci in usual interstitial pneumonia and non-specific interstitial pneumonia. *Respirology.* **2013**, *18*, 278−83.
(47) Silverstein, R. M.; Bassler, G. C. Spectrometric identification of organic compounds. *J. Chem. Educ.* **1962**, *39*, 546.
(48) Kiratipaiboon, C.; Stueckle, T. A.; Ghosh, R.; Rojanasakul, L. W.; Chen, Y. C.; Dinu, C. Z.; Rojanasakul, Y. Acquisition of cancer stem cell-like properties in human small airway epithelial cells after a long-term exposure to carbon nanomaterials. *Environ. Sci.: Nano* **2019**, *6*, 2152−70.
(49) MacPhail, R.; Strauss, H.; Snyder, R.; Elliger, C. Carbon-hydrogen stretching modes and the structure of n-alkyl chains. 2. Long, all-trans chains. *J. Phys. Chem.* **1984**, *88*, 334−41.
(50) Stone, K. C.; Mercer, R. R.; Gehr, P.; Stockstill, B.; Crapo, J. D. Allometric relationships of cell numbers and size in the mammalian lung. *Am. J. Respir. Cell Mol. Biol.* **1992**, *6*, 235−43.
(51) Pardo, A.; Cabrera, S.; Maldonado, M.; Selman, M. Role of matrix metalloproteinases in the pathogenesis of idiopathic pulmonary fibrosis. *Respir. Res.* **2016**, *17*, 23.
(52) Roeb, E. Matrix metalloproteinases and liver fibrosis (translational aspects). *Matrix Biol.* **2018**, *68*, 463−73.
(53) Dayer, C.; Stamenkovic, I. Recruitment of Matrix Metalloproteinase-9 (MMP-9) to the Fibroblast Cell Surface by Lysyl Hydroxylase 3 (LH3) Triggers Transforming Growth Factor-beta (TGF-beta) Activation and Fibroblast Differentiation. *J. Biol. Chem.* **2015**, *290*, 13763−78.
(54) El Agha, E.; Kramann, R.; Schneider, R. K.; Li, X.; Seeger, W.; Humphreys, B. D.; Bellusci, S. Mesenchymal Stem Cells in Fibrotic Disease. *Cell stem cell.* **2017**, *21*, 166−77.
(55) Levina, V.; Marrangoni, A. M.; DeMarco, R.; Gorelik, E.; Lokshin, A. E. Drug-selected human lung cancer stem cells: cytokine network, tumorigenic and metastatic properties. *PLoS One* **2008**, *3*, No. e3077.
(56) Vassalli, G. Aldehyde dehydrogenases: Not just markers, but functional regulators of stem cells. *Stem Cells Int.* **2019**, *2019*, 1.
(57) Ahmed Laskar, A.; Younus, H. Aldehyde toxicity and metabolism: the role of aldehyde dehydrogenases in detoxification, drug resistance and carcinogenesis. *Drug Metab. Rev.* **2019**, *51*, 42−64.
(58) Ahadome, S. D.; Abraham, D. J.; Rayapureddi, S.; Saw, V. P.; Saban, D. R.; Calder, V. L.; Norman, J. T.; Ponticos, M.; Daniels, J. T.; Dart, J. K. Aldehyde dehydrogenase inhibition blocks mucosal fibrosis in human and mouse ocular scarring. *JCI insight.* **2016**, *1*, No. e87001.
(59) Higashikuni, Y.; Sainz, J.; Nakamura, K.; Takaoka, M.; Enomoto, S.; Iwata, H.; Sahara, M.; Tanaka, K.; Koibuchi, N.; Ito, S.; Kusuhara, H.; Sugiyama, Y.; Hirata, Y.; Nagai, R.; Sata, M. The ATP-binding cassette transporter BCRP1/ABCG2 plays a pivotal role in cardiac repair after myocardial infarction via modulation of microvascular endothelial cell survival and function. *Arterioscler., Thromb., Vasc. Biol.* **2010**, *30*, 2128−35.
(60) Li, Y.; Jiang, D.; Liang, J.; Meltzer, E. B.; Gray, A.; Miura, R.; Wogensen, L.; Yamaguchi, Y.; Noble, P. W. Severe lung fibrosis requires an invasive fibroblast phenotype regulated by hyaluronan and CD44. *J. Exp. Med.* **2011**, *208*, 1459−71.
(61) Marriott, S.; Baskir, R. S.; Gaskill, C.; Menon, S.; Carrier, E. J.; Williams, J.; Talati, M.; Helm, K.; Alford, C. E.; Kropski, J. A.; Loyd, J.; Wheeler, L.; Johnson, J.; Austin, E.; Nozik-Grayck, E.; Meyrick, B.; West, J. D.; Klemm, D. J.; Majka, S. M. ABCG2pos lung mesenchymal stem cells are a novel pericyte subpopulation that contributes to fibrotic remodeling. *Am. J. Physiol Cell Physiol.* **2014**, *307*, C684−C98.
(62) Chang, S. H.; Yeh, Y. H.; Lee, J. L.; Hsu, Y. J.; Kuo, C. T.; Chen, W. J. Transforming growth factor-beta-mediated CD44/STAT3 signaling contributes to the development of atrial fibrosis and fibrillation. *Basic Res. Cardiol.* **2017**, *112*, 58.
(63) Kuwahara, G.; Hashimoto, T.; Tsuneki, M.; Yamamoto, K.; Assi, R.; Foster, T. R.; Hanisch, J. J.; Bai, H.; Hu, H.; Protack, C. D.; Hall, M. R.; Schardt, J. S.; Jay, S. M.; Madri, J. A.; Kodama, S.; Dardik, A. CD44 Promotes Inflammation and Extracellular Matrix Production During Arteriovenous Fistula Maturation. *Arterioscler., Thromb., Vasc. Biol.* **2017**, *37*, 1147−56.
(64) Wee, B.; Pietras, A.; Ozawa, T.; Bazzoli, E.; Podlaha, O.; Antczak, C.; Westermark, B.; Nelander, S.; Uhrbom, L.; Forsberg-Nilsson, K.; Djaballah, H.; Michor, F.; Holland, E. C. ABCG2 regulates self-renewal and stem cell marker expression but not tumorigenicity or radiation resistance of glioma cells. *Sci. Rep.* **2016**, *6*, 1−9.
(65) Torres-Padilla, M. E.; Chambers, I. Transcription factor heterogeneity in pluripotent stem cells: a stochastic advantage. *Development* **2014**, *141*, 2173−81.
(66) De Kumar, B.; Parker, H. J.; Parrish, M. E.; Lange, J. J.; Slaughter, B. D.; Unruh, J. R.; Paulson, A.; Krumlauf, R. Dynamic regulation of Nanog and stem cell-signaling pathways by Hoxa1 during early neuro-ectodermal differentiation of ES cells. *Proc. Natl. Acad. Sci. U. S. A.* **2017**, *114*, 5838−45.

https://dx.doi.org/10.1021/acsbiomaterials.0c00887
ACS Biomater. Sci. Eng. 2020, 6, 5290−5304

(67) Ambade, A.; Satishchandran, A.; Szabo, G. Alcoholic hepatitis accelerates early hepatobiliary cancer by increasing stemness and miR-122-mediated HIF-1α activation. *Sci. Rep.* **2016**, *6*, 21340.
(68) Grant, C.; Chudakova, D. A.; Itinteang, T.; Chibnall, A. M.; Brasch, H. D.; Davis, P. F.; Tan, S. T. Expression of embryonic stem cell markers in keloid-associated lymphoid tissue. *J. Clin. Pathol.* **2016**, *69*, 643−6.
(69) Zhang, H.; Yue, H.; Wang, C.; Hu, W.; Gu, J.; He, J.; Fu, W.; Hu, Y.; Li, M.; Zhang, Z. Clinical characteristics and the identification of novel mutations of COL1A1 and COL1A2 in 61 Chinese patients with osteogenesis imperfecta. *Mol. Med. Rep.* **2016**, *14*, 4918−26.
(70) Györfi, A. H.; Matei, A.-E.; Distler, J. H. Targeting TGF-β signaling for the treatment of fibrosis. *Matrix Biol.* **2018**, *68*, 8−27.

https://dx.doi.org/10.1021/acsbiomaterials.0c00887
ACS Biomater. Sci. Eng. 2020, 6, 5290−5304